TURBULENT FLOWS RESPONDING TO LOCAL BEHAVIORS OF BUOYANT BUBBLES

Yasuo Niida[1] and Yasunori Watanabe[2]

Abstract

In this study, physical relations between buoyant bubble behaviors and turbulent flows modified around bubbles were experimentally and computationally investigated with the aim to find out mechanical interactions occurring in bubble-laden turbulence as a model of aerated surf zone. It was found that the additional turbulence is locally intensified according to local motion of large bubbles, and the bubble induced turbulence enhances fluctuations of the bubble velocity. It is also found that turbulent fluid motion changes the bubble form and the orientation of bubble movement, resulting in fluctuating bubble motion which recursively produces additional turbulence. A stochastic bubble model was used to describe the local bubble motion in the turbulent flow in order to examine mechanical contributions of the bubble parameters.

Key words: air-bubbles, turbulence, PIV, back-light measurement, stochastic bubble model

1. Introduction

In a surf zone, wave crest overturn and plunge onto forward water, resulting in strong turbulence and air bubbles entrained underwater. Organized vortices formed during the splashing procedure of plunging waves involve and trap a large amount of bubbles, causing highly aerated complex flow field (Watanabe et al., 2005). The fine bubbles tend to be passively transported in turbulent flows and stay in the seawater for a longer time since a drag force is subject to the bubble motion rather than buoyancy, while larger bubbles rise with higher velocity and rapidly arrive at the surface owing to higher buoyancy. These differences in the relative velocity between bubbles and fluid characterize properties of bubbly flows and turbulence modified due to the bubble drag. The interaction between bubbles and turbulence is an important factor in determining local fluid motion that affects sediment transport, air-sea gas exchange, production of aerosol and other process in the surf zone.

There have been many studies on bubbly flow (e.g. Lance and Bataille, 1991). The bubbles entrained in the surf zone exhibit complex behaviors in strong turbulence (Ryu et al. 2005). While statistical properties of the bubble size under breaking waves have been studied by Deane and Stokes (2001) and Mori et al. (2007), dynamic effects of the bubble size distribution to turbulent flow field have not been understood. The authors (2010) numerically simulated local bubble behaviors based on a combination of Langevin equation and BBO bubble models, and found recursive dynamic process in the bubble flow; bubbles produce additional turbulence due to the bubble drag and the amplified turbulence yields fluctuations of the bubble velocity. The modified bubble motion additionally induces further fluctuations of the turbulent flow.

In this study, physical relations between buoyant bubble behaviors in turbulent flows and mechanical contributions of bubble deformation to turbulence are experimentally and computationally investigated with the aim to find out mechanical interactions occurring in bubble-laden turbulence. The final goal of this study is to understand mechanical contributions of air-bubbles involved in breaking-wave turbulence.

This paper is organized as follows. In Section 2, the experimental set-up and our imaging techniques to measure both of the bubble and fluid velocities are interpreted. A stochastic model used for examining mechanical contributions of the bubble parameters is explained in Section 3. The experimental and numerical results are described in Section 4, and they are summarized in Section 5.

[1]Hokkaido University, North 13 West 8, Spaooro 060 8628, Japan. niida@eng.hokudai.ac.jp
[2]Hokkaido University, North 13 West 8, Spaooro 060 8628, Japan. yasunori@eng.hokudai.ac.jp

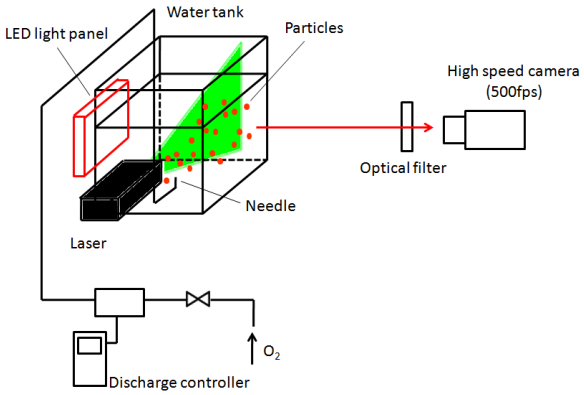

Figure 1. Experimental setup.

Table 1. Experimental conditions.

Case	Needle diameter d (mm)	Oxygen flow rate q (mL/min)
1	0.26	15
2	0.4	40
3	1.2	50
4	1.2	80
5	1.2	120

2. Experiment

A bubble plume was formed in a quiescent water pool. Oxygen was sent from a gas discharge controller through a needle fixed at the bottom of a rectangle transparent water tank (see Fig. 1). The bubble size and frequency of bubble ejection from the needle were controlled by changing the discharge of gas, q (in the range of 15 to 120 ml/min) and the needle diameter, d (from 0.26 to 1.2 mm), as shown in Table 1. Two different experiments were performed; back-light imaging experiment to acquire both of the geometric properties of bubbles, and Super Resolution Particle Imaging Velocimetry (SRPIV) measurement of fluid flow around the bubbles. The bubble-turbulence local interactions, via bubble deformation, fluctuations of bubble trajectory, generation of fluid turbulence and dispersion of the bubble, can be estimated during the both experiments. Details of the both experiments are described below.

2.1. *Detection of the Bubbles*

A LED light panel was attached on the back wall of water tank to record the shadows of the buoyant bubbles by a high-speed video camera (see Fig. 1). The size and displacement of the bubbles were estimated by detecting edges of the bubble shadows on the basis of a level-set edge detection technique (Watanabe et al., 2009). This method is based on a minimum fitting energy algorithm, which is outlined below.

The fitting term (F) for image intensity $g(x)$ is defined by

$$F = \int |g(x) - C_i|^2 H(\phi) dx + \int |g(x) - C_0|^2 (1 - H(\phi)) dx \quad (1)$$

where $H(\phi)$ is the numerical Heaviside function with boundary width ε:

$$H = \begin{cases} 0 & (\phi < -\varepsilon) \\ \frac{1}{2} + \frac{\phi}{2\varepsilon} + \frac{1}{2\pi}\sin(\pi\phi/\varepsilon) & (-\varepsilon \le \phi \le \varepsilon) \\ 1 & (\varepsilon < \phi) \end{cases} \tag{2}$$

where C_i and C_0 are the mean image intensities inside and outside the boundary, respectively. The level-set function, $\phi(x)$, is defined to indicate the signed distance from the edge boundary, and the shadow edges where $\phi = 0$ are determined to minimize Eq. (1). Thus, a level-set representation to minimize the fitting term, with additional constraint on the length, is written by

$$\frac{\partial \phi}{\partial t} = \delta(\phi)\{\mu\kappa(\phi) - \alpha\int |g - C_i|^2 H(\phi)dx + \beta\int |g - C_0|^2 (1 - H(\phi))dx \tag{3}$$

where μ, α, β are constants. δ and κ are numerical delta function and curvature, respectively. The level-set function ϕ for the image can be determined through iterative computation of Eq. (3). The bubble diameter, area and oblateness is determined by using geometric relations of the estimated bubble edges. The bubble velocity is simply estimated by tracking the centroid of the bubble.

2.2. *Super Resolution Particle Image Velocimetry (SRPIV)*

A SRPIV was introduced to measure distributions of local fluid velocity around the bubble plume. In this experiment, a YAG laser light sheet was installed from the side of the tank to illuminate neutral buoyant fluorescent particles mixed in the water. The displacement of the fluorescent particles was recorded by a high speed camera. Reflected lights of the laser at the bubbles surface were filtered out by a high-pass optical filter attached on the camera.

SRPIV is a hybrid version of particle image velocimetry (PIV) and particle tracking velocimetry (PTV) (Keane et al., 1995). A standard cross correlation PIV measurement is used to estimate interrogation window-scale velocity, and then the identical particle path following the window-scale velocity is searched over three sequential images on the basis of a minimum acceleration principal.

The statistical flow properties based on time-averaging are defined; mean velocity $\langle \boldsymbol{u} \rangle = (\langle u_f \rangle, \langle v_f \rangle)$, and turbulent kinetic energy, $k = \left(u_f'^2 + v_f'^2\right)/2$, where u_f' and v_f' are fluctuating components of instantaneous velocity $\boldsymbol{u} = \langle \boldsymbol{u} \rangle + \boldsymbol{u}_f$'.

3. Stochastic Bubble Model

In order to examine mechanical contributions of the bubble parameters, stochastic turbulence model is introduced to model the local bubble motion. A Lagrangian representation of fluid drift and diffusion processes in turbulent flows in a framework of the stochastic approach (see details in Pope, 2000) has been extended to the particle-laden turbulent flows (Guingo and Minier, 2008). This approach, coupled with Eulerian Large Eddy Simulation, is also applied to the bubble flows (Niida et al. 2010).

The bubble motion is expressed by well-known Basset-Bousinesq-Oseen (BBO) equation:

$$\frac{dx_i^p}{dt} = u_i^p \tag{4}$$

$$\frac{du_i^p}{dt} = \frac{u_i^s - u_i^p}{\tau_p} + \frac{\rho_f}{\rho_p}\frac{Du_i^s}{Dt} + \frac{C_a}{2}\frac{\rho_f}{\rho_p}\left(\frac{du_i^s}{dt} - \frac{du_i^p}{dt}\right) + \left(1 - \frac{\rho_f}{\rho_p}g_i\right) \tag{5}$$

Here, x^p is the bubble location, u^p is the bubble velocity, and ρ_f is the fluid density. ρ_p is the density of air, C_a is the added mass coefficient, g is the gravity and u^s is the instantaneous fluid velocity at x^p. The Basset term is assumed to be negligibly small. The relaxation time τ_p is defined by

$$\tau_p = \frac{\rho_p}{\rho_f}\frac{4d}{3C_D\left|u^s - u^p\right|} \tag{6}$$

where C_D is the drag coefficient. Since C_D generally depends on deformation of bubbles, the following drag C_D, proposed by Peebles and Garber (1953), was used.

$$C_D = \max\left[\max\left[\frac{24}{\mathrm{Re}}, \frac{18.7}{\mathrm{Re}^{0.68}}\right], \min\left[0.0275M\,\mathrm{Re}^4, 0.82M^{0.25}\,\mathrm{Re}\right]\right] \tag{7}$$

where *Re* is particle Reynolds number, and *M* is Morton number.

A Langevin equation model (Pope, 2001) was used to determine fluid velocity at the bubble location u_s. The general form of the Langevin model is written by

$$du_i^s = A_{s,i}dt + B_{s,i}dW_i \tag{8}$$

where $A_{s,i}$ is the drift vector, $B_{s,i}$ is the diffusion matrix and W_i is a vector-valued Wiener process. According to Guingo and Minier (2008), $A_{s,i}$ and $B_{s,i}$ can be expressed by

$$A_{s,i} = -\frac{1}{\rho_f}\frac{\partial\langle p\rangle}{\partial x_i}dt + \left(\left\langle u_i^p\right\rangle - \left\langle u_i^f\right\rangle\right)\frac{\partial\left\langle u_i^f\right\rangle}{\partial x_j}dt - \frac{u_i'^s}{T_{L,i}^*}dt + g_i dt \tag{9}$$

$$B_{s,i} = \sqrt{\langle\varepsilon\rangle\left(C_o\frac{T_L}{T_{L,i}^*} + \frac{2}{3}\left(\frac{T_L}{T_{L,i}^*} - 1\right)\right)} \tag{10}$$

where p is the pressure, T_L* are the Lagrangian time scale with a so-called crossing trajectory effect (Csanady, 1963). u'^s_i is fluctuating velocity of u_s.

$$T_{L,1}^* = \frac{T_L}{\sqrt{1 + \beta^2\left|\langle u_r\rangle\right|^2 / (2k/3)}} \tag{11}$$

$$T_{L,3}^* = \frac{T_L}{\sqrt{1 + 4\beta^2\left|\langle u_r\rangle\right|^2 / (2k/3)}} \tag{12}$$

where T_L is the Lagrangian integral time scale

$$T_L = \frac{1}{1/2 + 3/4Co}\frac{k}{\varepsilon} \tag{13}$$

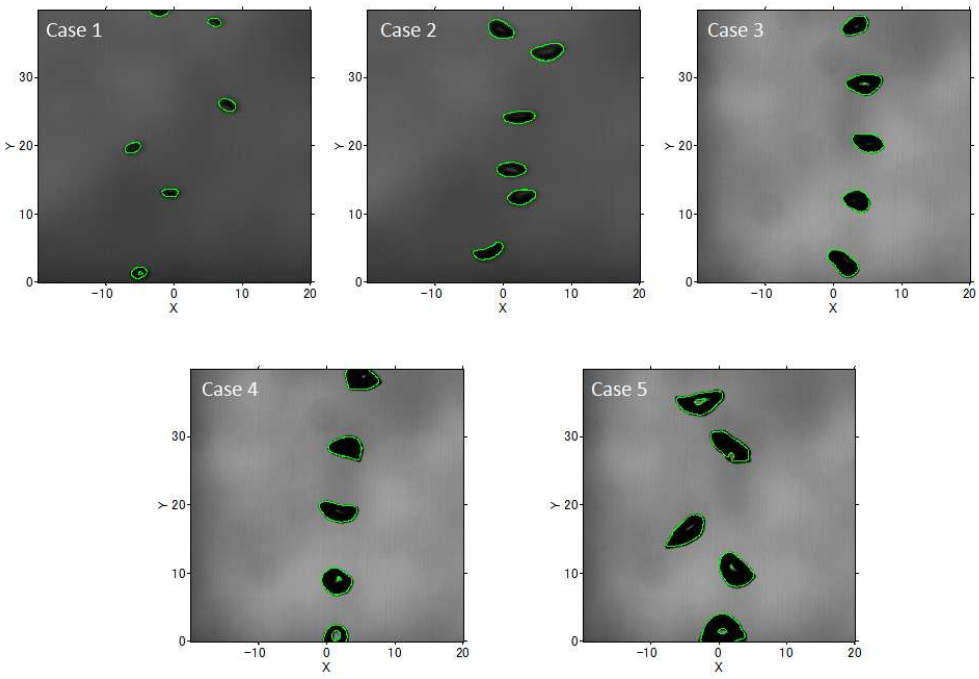

Figure 2. Typical back-light images of bubbles and the detected bubble edges.

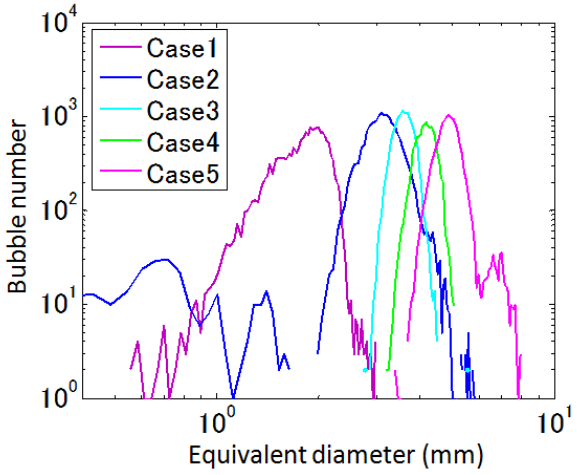

Figure 3. Bubble size spectrum.

The local bubble behaviors, responding to turbulent flow measured by SRPIV, are numerically simulated to find out mechanical contributions in bubble-turbulence interactions.

4. Results

Figure 2 shows the typical back-light images of bubbles and the detected bubble edges. It is seen that size and shape of the bubbles have been controlled with air flow discharge. The bubble size spectrum (for the diameter of a circle with the same area of the deformed bubble) is shown in Fig. 3. The maximum spectrum appears at the equivalent diameters of 2.0, 3.1, 3.6, 4.2, and 4.9 mm for cases 1 to 5. The same number of

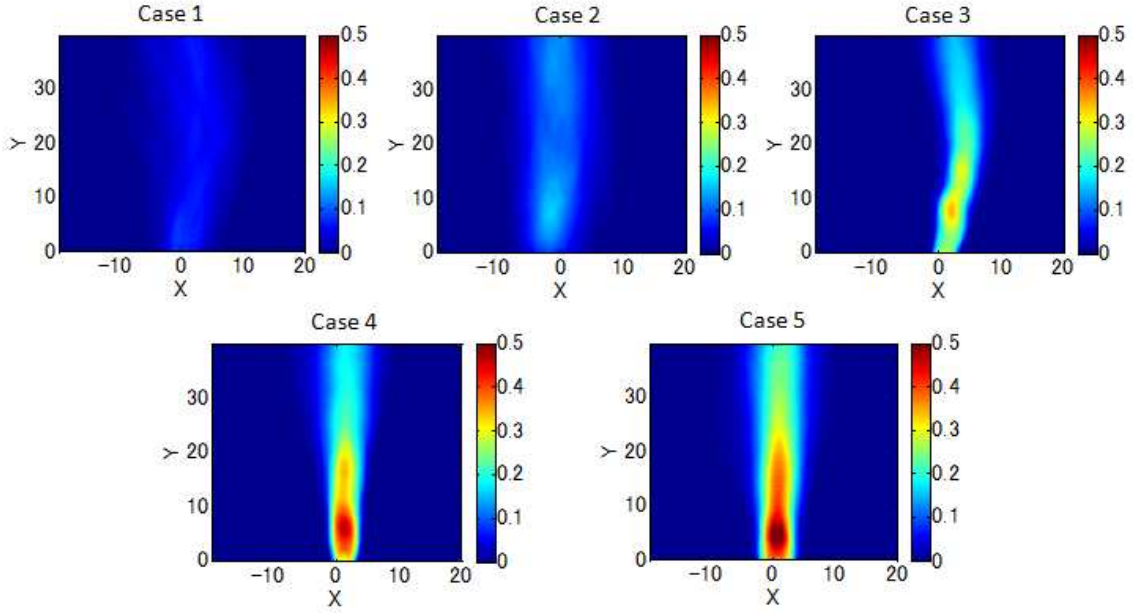

Figure 4. Distributions of the mean void fraction

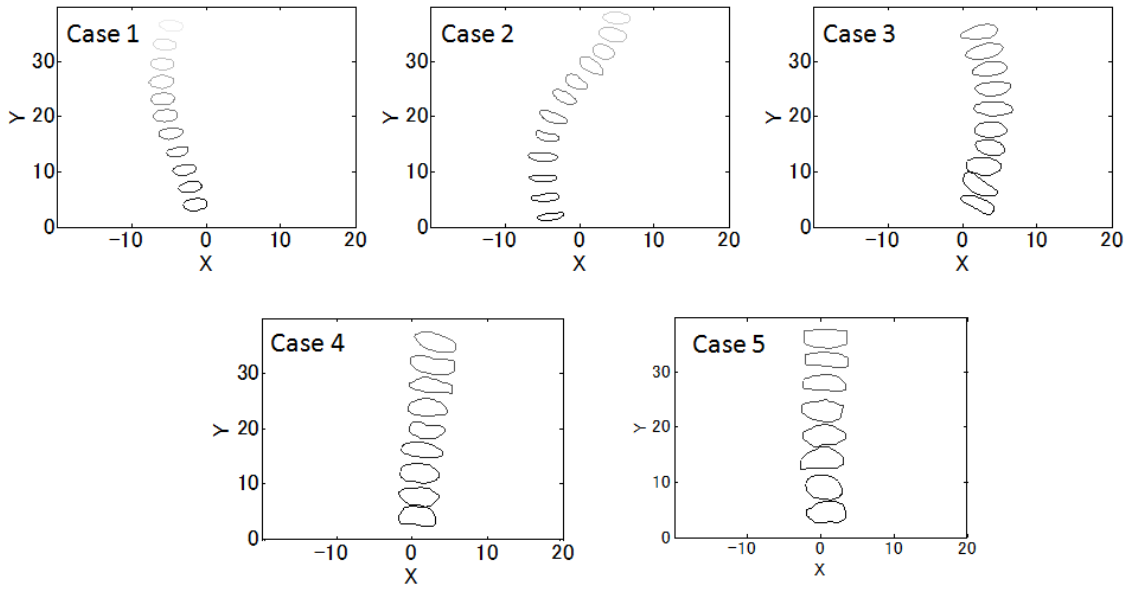

Figure 5. Bubble shapes along the bubble trajectories

the bubbles with the uniform size was ejected in each experiment.

The distribution of mean void fraction are shown in Fig. 4. Because of the same bubble number density for all cases, higher mean void fractions are observed for larger bubble cases. The vertically decrease of the void fraction indicates lateral dispersions of the buoyant bubbles. Figure 5 shows the bubble shapes varying with local movements of the bubbles. In cases 1 – 3 with typical zigzag trajectories, lateral surface deformation is observed to be synchronized with change in orientation of the bubble motion. Larger bubbles tend to rise with less lateral displacement (see cases 4 and 5), while the bubble shape rapidly varies

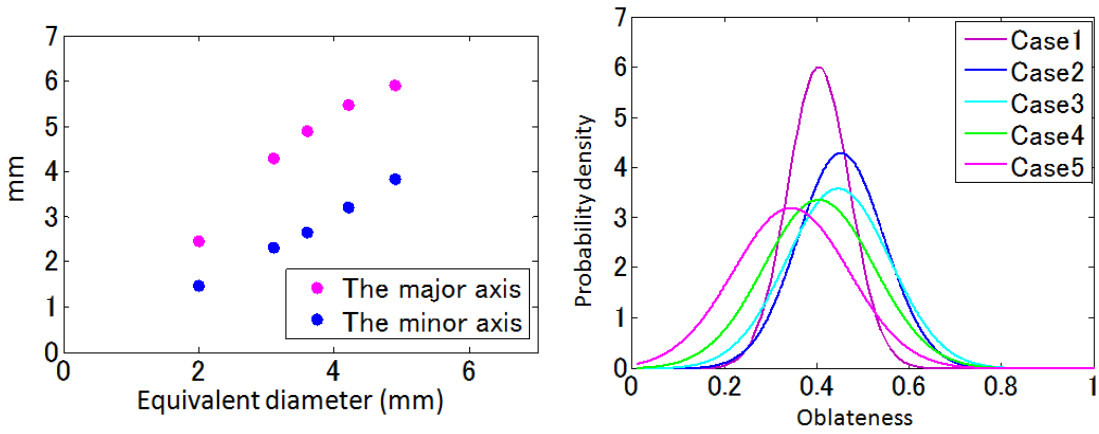

Figure 6. Ellipse semi-axes (left) and probability density distributions of oblateness of the bubble

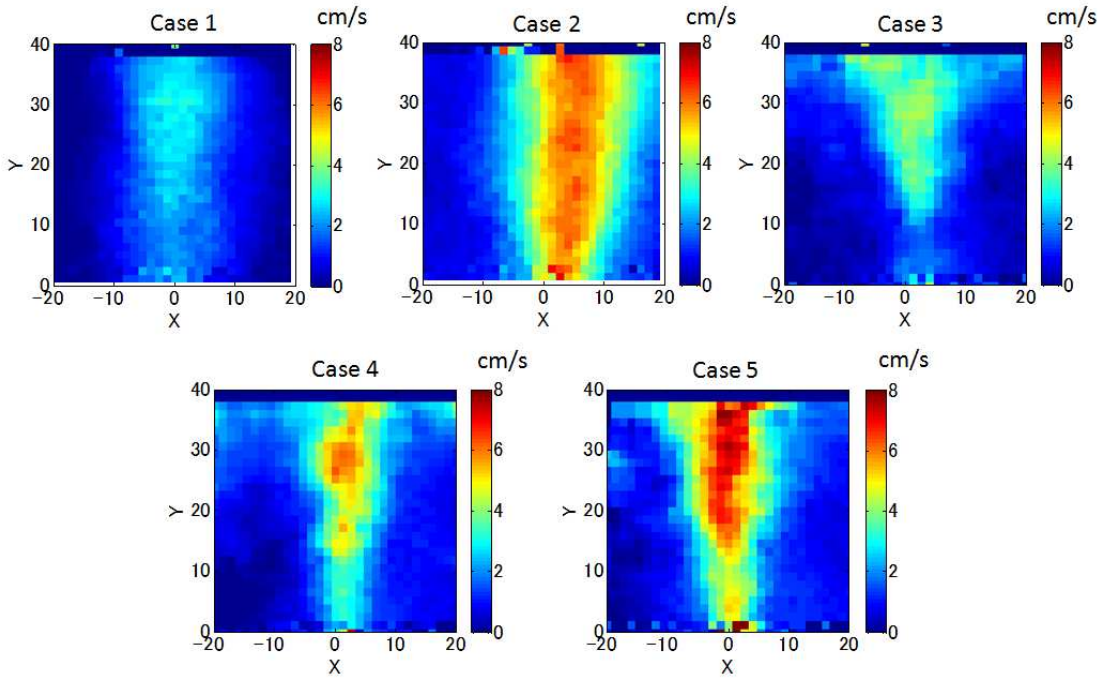

Figure 7. Spatial distributions of mean vertical fluid velocity.

at every time frame.

When the bubble shape is assumed to be ellipse, mean major, *a*, and minor axes, *b*, of the ellipse with the same area of the bubble can be defined (see Fig. 6). The probability density of oblateness, defined by *oblateness=1-b/a*, indicates that the mean oblateness decreases and the dispersion increases with the bubble size; that is, local surface deformation of larger bubbles rapidly changes during the buoyant process.

The measured fluid vertical velocity in the bubble plume is shown in Fig. 7. It is observed that the fluid flow is accelerated due to the drag force induced by the bubble rise. While the void fraction, shown in Fig. 4, is known to be one of the parameters charactering bubble flow, there is no explicit correlation with the fluid flow.

Figure 8 shows the spatial distribution of the measured fluid turbulent energy. Relatively high turbulent

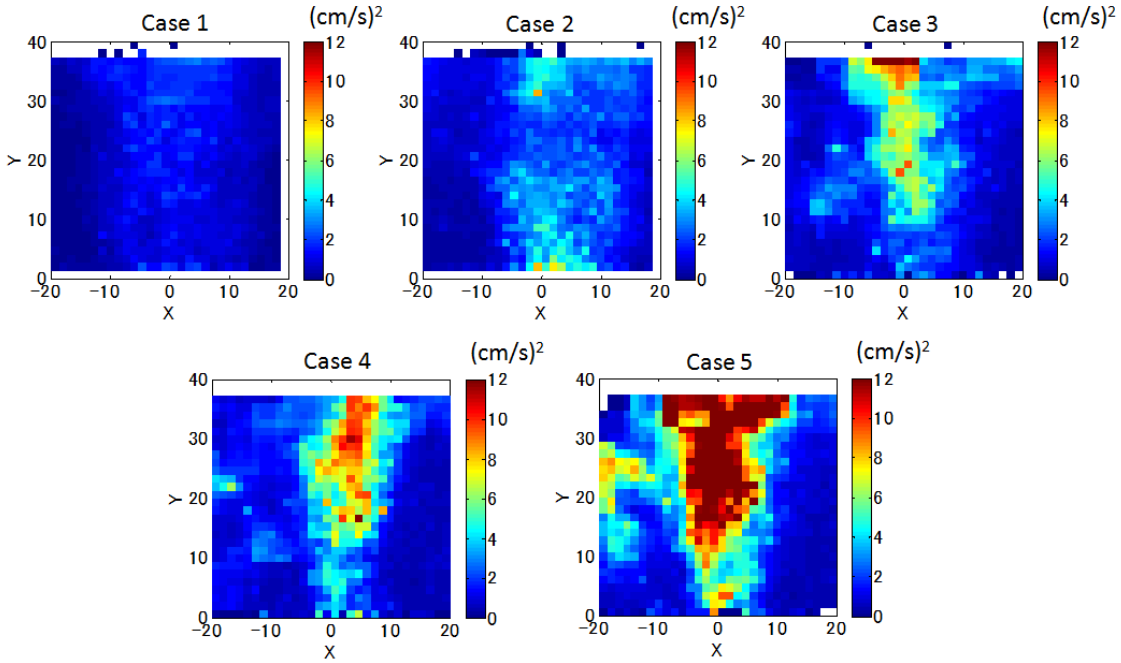

Figure 8. Spatial distributions of fluid turbulent energy.

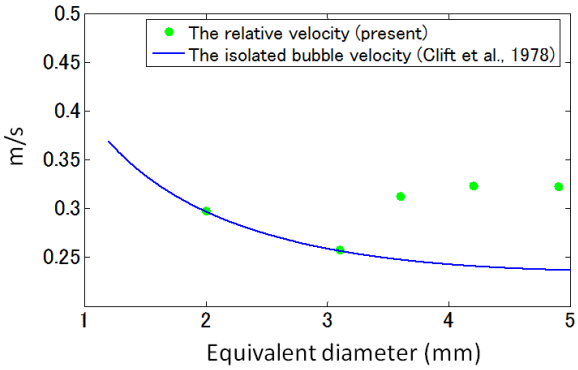

Figure 9. Comparisons of the relative velocity with the isolated rise velocity by Clift et al. (1978).

energy is observed in larger bubble cases (cases 4 and 5), while there is less correlation with the mean void fraction (see also Fig. 4). It is known that bubbles in flows can intensify the fluid turbulence around them (e.g. Bunner and Tryggvason 2002) or suppress it, depending on the relative size of the bubble and the turbulence length-scale (Gore and Crowe 1989). The bubble-induced vertical fluid velocity forms shearing flows around the bubble plume, and the shear-induced turbulence may be suppressed by small bubbles (cases 1 and 2) and intensified by larger bubbles (cases 3-5). Although the void fraction has been used as a parameter for modeling mechanical stress due to the presence of bubble, the current results indicate that local turbulence needs to be determined with additional parameters. The bubble-intensified turbulence contributes to change the bubble form and motion, which is discussed below.

Figure 9 shows the comparison of the measured mean rise relative velocity in the plume with the isolated single bubble relative velocity (Clift et al. 1978). Our results for smaller bubble cases (1 and 2)

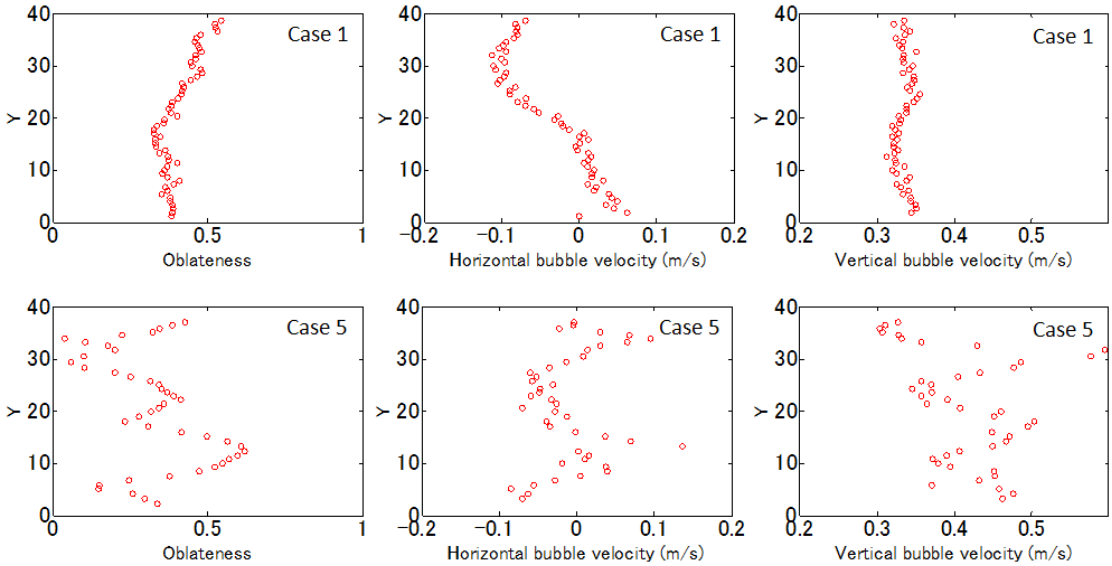

Figure 10. Vertical distribution of the oblateness of the bubble (left) , horizontal bubble velocity (middle) and vertical bubble velocity(right).

coincide with the single bubble one, and therefore the bubble drag in these cases is identical with the single bubble case. On the other hand, significant deviations can be found in the other cases 3, 4 and 5 in which significant turbulence intensification occurs (see also Fig. 8). This suggests that interconnected mechanics between the drag due to local bubble behaviors and turbulence.

Figure 10 shows the vertical distribution of the oblateness, the horizontal and vertical bubble velocities. In case 1, because of less turbulence, there are smooth variations in bubble velocity following changes in the bubble shape during the bubble lifetime. However, in case 5, the oblateness rapidly changes, and the both horizontal and vertical bubble velocities also change with amplitude of 10 cm/s that is comparable to the bubble-induced vertical velocity (see also Fig. 7). That is, turbulent fluid motion changes the bubble form and the orientation of bubble movement, resulting in fluctuating bubble motion which recursively produces additional turbulence. This recursive interactions between bubbles and turbulence are interpreted by using numerical tests, discussed below.

The mechanical contributions of turbulence to bubble fluctuations are examined through numerical tests using BBO and Langevin models described in Section 3. The probability density distributions of the computed and experimental rise velocity are compared in Fig. 11. High correlation can be observed for small bubble cases (with less deformation), indicating that the mechanical effects of fluid turbulence reasonably provides to the bubble velocity fluctuations in the current model. For larger bubbles, however, since the model assumes a spherical bubble, effects of the bubble deformation resulted from the fluid turbulence to the bubble motion cannot be reproduced by this model. This effect causes significant discrepancies of the computed bubble velocity statistics with the experimental one in larger bubble cases.

The fluid turbulent diffusion coefficient, D_T, is defined in a framework of the Langivan model as

$$D_T = \frac{1}{2} B_s^{\,2} \tag{14}$$

Figure 12 shows the turbulent diffusion and the root-mean-squares (rms) of computed and experimental bubble velocities. The both of computed diffusion and rms velocity monotonically increase with the bubble equivalent diameter, indicating our model reasonably provide the effect of fluid turbulence to the bubble fluctuating behavior. However, the overestimated experimental rms bubble velocity with respect to

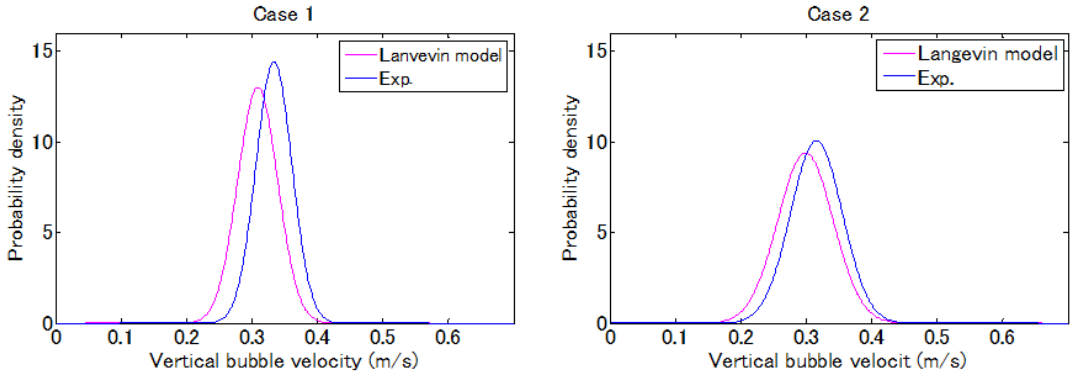

Figure 11. The probability density distributions of the rise bubble velocity

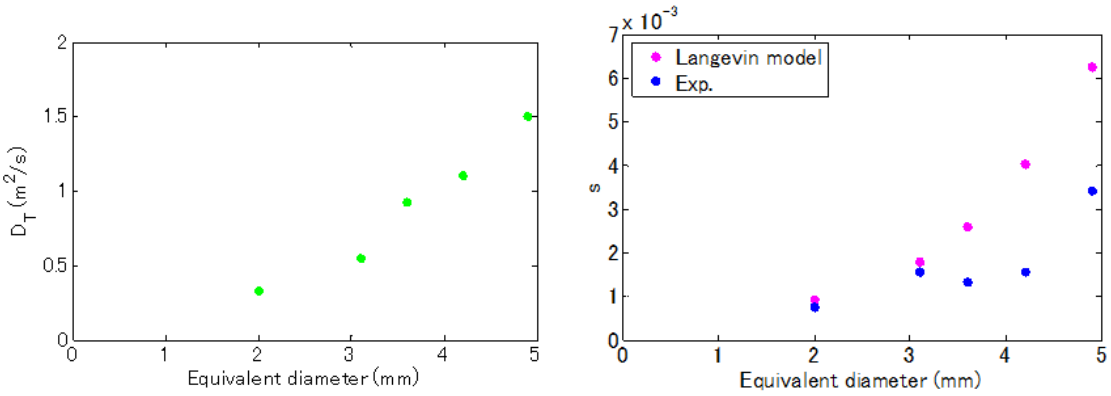

Figure 12. Turbulent diffusion coefficient (left) and rms of bubble velocity (right)

the computed one suggests poor reproducibility due to lack of a mechanical model for the bubble deformation. That suggests that the turbulence-induced deformation of bubbles and the bubble velocity fluctuations due to the bubble deformation are crucial factors to reproduce bubble-laden flows.

In the surf zone, various sized bubbles, ranging in O (10μm-10mm), are involved in wave-breaking turbulence. There may be turbulence amplification or suppression due to the entrained bubbles, depending on the bubble size. Additional turbulence may be induced by the local bubble velocity fluctuations via rapid and consecutive deformation resulted from the fluid turbulence. This recursive local interaction between the bubble and turbulence should be taken into account to establish a reasonable model to reproduce realistic babble-laden turbulent flows under breaking waves.

5. Conclusions

Physical relationship between buoyant bubble behaviors and turbulence were experimentally and computationally investigated.

Image measurements for the bubbles and liquid velocity field confirmed that the shear-induced turbulence is suppressed by small bubbles and intensified by larger bubbles. Although mean void fraction has been usually used as a parameter for modeling mechanical stress due to the bubbles, this results indicate that local turbulence needs to be determined with additional parameters.

Measurements of relative velocity in bubble plume was larger than the velocity of isolated single

bubble in cases with large bubbles. That is because of the interconnected mechanics between the drag due to local bubble behaviors and turbulence. The intensified turbulence also caused temporal variation of the oblateness and the bubble velocity. These fluctuations of the bubble shape and velocity recursively produced additional turbulence.

A stochastic bubble model was used to describe the local bubble motion in the turbulent flow and compared with the present experimental ones. Although the velocity field of the bubble plume agreed well with the experimental results with small bubbles, the velocity field deviated from the experimental results with large bubbles. The turbulence-induced deformation of bubbles and the bubble velocity fluctuations due to the bubble deformation are important factors for bubble-laden flows. The recursive interaction between the bubbles and turbulence should be taken into account to establish a reasonable model to reproduce the babble-laden turbulent flow in the surf zone.

Acknowledgements

Financial support for this study was provided by JSPS Research Fellowships for Young Scientists

References

Bunner, B., Tryggvason, G., 2002. Dynamics of homogeneous bubbly flows Part 2. Velocity fluctuations. *Journal of Fluid Mechanics* Vol.466, 53-84.

Csanady, G. T., 1963. Turbulent diffusion of heavy particles in the atmosphere. *J. Atmos. Sci.*, 20 (3), 201-208.

Deane, G. B., and Stokes, M. D., 2002. Scale dependence of bubble creation mechanisms in breaking waves. *Nature*, 418, 840-844.

Gore R.A. and Crowe C.T., 1989. Effect of particle size on modulating turbulent intensity. *Int. J. Multiphase Flow*, Vol.15, 279-285.

Guingo, M. and Minier, J. P., 2008. A stochastic model of coherent structures for particle deposition in turbulent flows. *Phys. Fluids*, 20, 053303.

Keane, R. D., Adrian, R. J. and Zhang, Y., 1995. Super-resolution particle imaging velocimetry. *Meas. Sci. Technol.*, 6, 754-768.

Lance, M. and Bataille, J., 1991. Turbulence in the liquid phase of a uniform bubbly air-water flow. *J. Fluid Mech*., 222, 95-118.

Mori, N., Suzuki, T., Kakuno, S., 2007. Experimental study of air bubbles and turbulence characteristics in the surf zone. *Journal of Geophysical Research*, 112, C05014.

Niida, Y., Mitobe, Y. and Watanabe, Y., 2010. LES-Stochastic coupling model of bubble-laden turbulence. *Proc. ISOPE*, 750-754.

Peebles, F. N. and Garber, H. J., 1953. Studies on the motion of gas bubbles in liquids. *Chem. Eng. Prog*, 49 (2), 88-97.

Pope, S. B., 2000. *Turbulent Flows*, Cambridge University Press

Ryu, Y., Chang, K.-A. and Lim, H.-J., 2005. Use of bubble image velocimetry for measurement of plunging wave impinging on structure and associated greenwater. *Meas. Sci. Technol.*, 16, 1945–1953.

Watanabe, Y. and Ishizaki S., 2009. Spray size distributions at flip-through wave overtopping. *Proc. Coastal Dynamic*.

Watanabe, Y., Hiroshi S. and Roger J. H., 2005. Three-dimensional vortex structures under breaking waves. *J. Fluid. Mec.*, 545, 291-328.